Protein Engineering vol.8 no.7 pp.663–675, 1995

Free energy simulations of the HyHEL-10/HEL antibody–antigen complex

R.Pomès[1,2,3], R.C.Willson[4] and J.A.McCammon[1,5]

[1]Department of Chemistry and [4]Department of Chemical Engineering and Department of Biochemical and Biophysical Sciences, University of Houston, Houston, TX 77204, USA

[2]Present address: Department of Chemistry, University of Montreal, CP 6128, Succ. A, Montreal (Quebec) H3C 3J7, Canada

[5]Present address: Department of Chemistry and Biochemistry and Department of Pharmacology, University of California at San Diego, La Jolla, CA 92093, USA

[3]To whom correspondence should be addressed

Free energy simulations are reported for the N31^{L}D mutation, both in the HyHEL-10–HEL antibody–lysozyme complex and in the unliganded antibody, using the thermodynamic-cycle perturbation method. The present study suggests that the mutation would change the free energy of binding of the complex by −5.6 kcal/mol (unrestrained free energy simulations), by −0.5 kcal/mol (free energy simulations with a restrained backbone) and by 1.8 kcal/mol (Poisson–Boltzmann calculations, which also use a restrained geometry model). A detailed structural analysis helps in estimating the contributions from various residues and regions of the system. Enhanced recognition of HEL by the mutant HyHEL-10 would arise from the combination of thermodynamically more favorable conformational changes of the CDR loops upon association and subsequent charge pairing with Lys96 in the antigen.

Key words: antibody–antigen complex/free energy simulations/single-point mutant/thermodynamic cycle

Introduction

The molecular recognition of large substrates is central to the immunological response. The recognition and binding of antibodies to antigenic molecular sites helps inactivate viruses and bacteria and initiates a succession of events that results in the destruction of foreign molecules. This process requires both a very highly selective discrimination in order that the integrity of the self be preserved and a dazzingly diverse response, so that virtually any non-self molecule can be identified. The elucidation of the 3-D structures of antibody–antigen complexes revealed that these properties arise from the association with a large number of antibody residues on an extended surface made up of as many as six antigen-binding loops whose primary sequence displays high variability (the hypervariable loops) (Alzari *et al.*, 1988).

The association of proteins is thought to result from thermodynamic forces involving a large number of intermolecular interactions that may be described as hydrogen bonds, van der Waals contacts and electrostatic interactions, purely entropic contributions such as those arising from the restriction of translational, rotational and internal conformational freedom upon association, and solvent effects. Whereas the nature and origins of these various factors are generally understood, their relative importance is a matter of current debate. For instance, Dill (1990) argues that hydrophobic forces dominate protein folding, but that ion pairing can also stabilize proteins, and he notes that the magnitude of hydrogen bonds and van der Waals interactions among polar amino acids remains poorly understood. A detailed understanding, however, is paramount to the effective development of protein engineering strategies, in protein folding and stability and molecular recognition problems alike (Novotny *et al.*, 1989; Sauer and Lim, 1992).

Among the techniques that can be used to probe the stability of protein–substrate interactions, site-directed mutagenesis offers wide prospects towards a detailed assessment of the factors at play in molecular recognition: the replacement of individual side chains potentially allows for very specific perturbations to the association. Thermodynamic measurements such as calorimetric measurements can then be used to determine the corresponding change in stability. In order to extract unambiguous information from such studies (Sauer and Lim, 1989), one needs detailed information on the nature of the physical changes induced by the point mutation. This is sometimes difficult to obtain in cases where structural information on the mutant protein is lacking, because significant conformational rearrangements may result from the mutation, which in turn can complicate predictions made with reference to the native state. In order to minimize this uncertainty, it may be preferable to choose mutations that conserve the general structure and activity of the native protein. In such cases, one might hope that small and localized changes in the physical properties of the mutant give rise to small and localized changes in the structure and affinity of the protein for its ligand.

Computer techniques appear well suited to address the problem of structure and affinity changes upon small modifications of macromolecules, because they allow one to monitor both effects on a microscopic scale. In particular, molecular dynamics simulations used in conjunction with free energy calculations are the technique of choice if one wants to monitor the results of a point mutation (Subramaniam *et al.*, 1989). Such methods have been developed and used successfully in a number of recent studies pertaining to the binding of ligands (Lee, 1992 and references therein; Straatsma and McCammon, 1992), including the effect of mutations on the free energy of dimerization of hemoglobin (Kuczera *et al.*, 1990), on the stability of T4 lysozyme (Prevost *et al.*, 1991) and barnase (Tidor and Karplus, 1991), and on the binding of tryptophan by the *trp* repressor (Komeiji *et al.*, 1992).

The work presented here attempts to extend the methodology to an antibody–antigen complex as an example of a protein–protein complex with a large interface. The engineered modification of antibodies is currently a very active field and research groups have reported successful attempts at fabricating antibodies with designed catalytic properties and human antibodies have been designed with mouse hypervariable loops (Presta, 1992 and references therein).

We present the application of free energy calculations to determine the relative antigen-binding affinity of a mutant antibody with respect to the wild type HyHEL-10 (Smith-Gill *et al.*, 1984). The crystal structure of that antibody's antigen binding fragment (Fab) complexed with its antigen protein, hen egg white lysozyme (HEL), has been solved (Padlan *et al.*, 1989). The purpose of the mutation considered, the replacement of an asparagine side chain, $Asn31^{L}$, by Asp, is to putatively introduce a salt link between that residue and the positively charged terminal of a lysine of lysozyme, $Lys96^{HEL}$, which is within contact distance in the crystallographic structure and appears to be shielded from solvent. The latter distinction is significant because electrostatic screening by water might weaken the ion pair. In fact, recent mutational studies of salt links on the surface of proteins converge to the conclusion that surface salt links contribute marginally to the stability of proteins (Horovitz *et al.*, 1990; Dao-Pin *et al.*, 1991). On the other hand, the weakening of a solvent-inaccessible salt link in HyHEL-5–HEL, another antibody–lysozyme complex, through replacement of $Arg48^{HEL}$ by Lys showed a 1000-fold loss in affinity (Lavoie *et al.*, 1989). Furthermore, the stability of the association of the constant domains of immunoglobulins has been found to correlate well with the number of buried salt bridges between them (Schiffer *et al.*, 1988).

Some care was taken in the solvation of our protein model. This is of importance since there are a number of possibly solvated cavities within the protein assembly and because buried waters can be of critical importance to the structure and activity of polypeptide molecules, as discussed in a computational study (Wade *et al.*, 1990, 1991) and a review article (Meyer, 1992). However, the crystallographic structure is of little help in the present case, since its resolution allows for the detection of only one water molecule (Padlan *et al.*, 1989). On the other hand, the association of the antibody Fab HyHEL-5 with hen egg lysozyme has been believed to result in large part from excellent complementarity that excludes interface water molecules (Sheriff *et al.*, 1988), an assumption that will be tested in the present system.

One of the factors likely to affect the thermodynamics of antibody–antigen binding is the extent of conformational rearrangement of the protein(s) upon association. The conventional view of antibody–antigen association regards it as a 'lock and key' process (Amit *et al.*, 1986), whereby the proteins are presented to each other in the conformation in which they will bind. Whereas this was inferred from the highly conserved sequence of most of the antigen-binding domains of antibodies (the variability of the so-called 'variable' domain being in fact essentially restricted to the hypervariable loops making up the complementarity-determining regions, or CDRs, that bind the antigen), evidence for some degree of adjustment of the antigen-binding regions upon complexation or 'induced-fit' has begun to emerge (Rini *et al.*, 1992 and references therein). One expects limited flexibility of the CDR loops, however, because a high degree of flexibility could in principle allow for non-specific recognition of various antigenic surfaces and would augment the entropic cost of binding, thus limiting both the specificity and affinity. Limited flexibility is, in turn, compatible with the concept of canonical structures (Chothia and Lesk, 1987). This assumption is essential to the current tractability of computational studies, since in order to allow for the convergence and accuracy of the free energy perturbations, all accessible conformations must be sampled during free energy calculations. Furthermore, we expect the specificity of the antibody to be very sensitive to the precise relative orientation of the CDR loops. The matter of CDR loop main chain conformations will therefore be addressed in some detail in the present study.

Finally, an outstanding problem concerns the treatment of long-range electrostatic interactions. This aspect of molecular dynamics calculations can be very demanding if the solvent molecules are included explicitly in the model. For that reason, alternatives to that approach have been sought. Among them, electrostatic continuum methods, in which the solvent is treated as a dielectric continuum, have been used recently in a number of calculations (Sharp and Honig, 1990; Honig *et al.*, 1993; Roush *et al.*, 1994). In particular, the application of continuum electrostatic theory to the calculation of the complexation energies of another antilysozyme antibody, HyHEL-5, with HEL, for a large number of single-point mutants (Slagle *et al.*, 1994), suggests that the method may be useful in the rational design of antibodies.

Materials and methods

Thermodynamic-cycle perturbation method

The thermodynamic cycle used to calculate the relative Helmholtz free energy of antigen-binding of a mutant Fab' with respect to the wild type Fab is depicted below.

$$\begin{array}{ccc} \text{Fab} + \text{Ag} & \xrightarrow{\Delta A_1} & \text{Fab/Ag} \\ \Delta A_3 \downarrow & & \downarrow \Delta A_4 \\ \text{Fab}' + \text{Ag} & \xrightarrow{\Delta A_2} & \text{Fab}'/\text{Ag} \end{array} \qquad (1)$$

The theoretical basis used for the calculation of $\Delta\Delta A = \Delta A_2 - \Delta A_1$ is the thermodynamic-cycle perturbation method (Tembe and McCammon, 1984), whereby $\Delta\Delta A$ is calculated as $\Delta A_4 - \Delta A_3$. Because the free energy is a state function, the two paths are equivalent in theory. Computationally, however, the latter path is preferred because it does not require the simulation of bottle-necks such as the lengthy diffusional encounter of the solutes and the desolvation which occurs upon docking (equations 1 and 2). Instead, the unphysical transformations represented by equations (3) and (4) correspond to the numerical substitution of the wild type residue by its mutant counterpart. On the assumption that both the wild type and the mutant antibody variable domains have the same folding, the calculations of ΔA_3 and ΔA_4 can be carried out with configurational sampling restricted to local changes at and around the site of the mutation in the unliganded and liganded cases respectively.

Two methods have been used extensively that allow computation of the free energy differences between a molecular system and a perturbed or mutated counterpart in the canonical ensemble (Beveridge and DiCapua, 1989; van Gunsteren and Berendsen, 1990; Straatsma and McCammon, 1991). In both approaches, a perturbation is introduced into a molecular dynamics simulation. The so-called 'perturbation method' computes the free energy difference as

$$\Delta A = -kT\ln[\langle e^{-\Delta H/kT}\rangle_0] \qquad (2)$$

where k is the Boltzmann constant, ΔH is the perturbation to the Hamiltonian of the system and the subscript indicates that

averages are computed in the reference (unperturbed) ensemble. Whenever the perturbation is large, it is desirable to break up the simulation into smaller successive perturbation calculations and subsequently sum up over such 'windows', in order to improve the accuracy of the averaging.

In the second method, often referred to as 'thermodynamic integration', the perturbed Hamiltonian is written as

$$H(\lambda) = (1 - \lambda)^n H(0) + \lambda^n H(1) \quad (3)$$

where n is an integer and λ, a perturbation parameter that varies from 0 to 1, gradually introduces the perturbation. Free energy changes are computed as summations over the ensemble-averaged derivative of the Hamiltonian with respect to λ. Thus, in the case of linear scaling (i.e. $n = 1$),

$$\Delta A = \int_0^1 < H(1) - H(0) >_\lambda \, d\lambda \approx \sum_{\lambda=0}^{1} < H(1) - H(0) >_\lambda \, \delta\lambda \quad (4)$$

Here, the right-hand side of the equation is a computable approximation for a finite number of successive integration steps separated by an increment $\delta\lambda$.

Decomposition of the free energy change

Whereas the two methods described above are equivalent in the limit of infinite sampling, the thermodynamic integration method with linear scaling offers the possibility of approximately separating individual contributions to the free energy change. That is, if $\Delta H = H(1) - H(0)$ is partitioned into a sum of components $\Sigma_i \Delta H^i = \Sigma_i \{H^i(1) - H^i(0)\}$, then equation (4) can be rewritten as

$$\Delta A = \sum_\lambda < \sum_i \Delta H^i >_\lambda \, \delta\lambda = \sum_i \sum_\lambda < \Delta H^i >_\lambda \, \delta\lambda = \sum_i \Delta A^i \quad (5)$$

where ΔA^i represents the contribution to the free energy change arising from the perturbation of H^i. It should be noted, however, that although A is a state function, the values of the ΔA^i terms are path dependent (Straatsma and McCammon, 1992; Mark and van Gunsteren, 1994). Therefore, contributions to ΔA should not be considered as physically exact values, but rather as an indication of the relative magnitude of contributions arising from different regions of the molecular system or, alternatively, from different terms used to describe the force field, in the particular path chosen for the perturbation.

Molecular dynamics simulations

This and the following sections describe successively the force-field used in the computations, the solvation and equilibration procedures and the perturbation calculations for Asn to Asp mutation in the HyHEL-10–HEL complex and in the unliganded antibody. Similar calculations were initially performed on a reference solvated dipeptide system. The dipeptide model with an Asn side chain is depicted in Figure 1 in the crystallographic conformation of residue 31^L.

The starting point for the simulations is provided by the crystallographic structure of the antigen binding fragment (Fab) of the antibody HyHEL-10 with its antigen, hen egg white lysozyme (HEL), solved at 3.0 Å resolution (Padlan *et al.*, 1989). The coordinates of the complex are available from the Brookhaven Protein Data Bank (Bernstein *et al.*, 1977). The methodology described in detail below was used

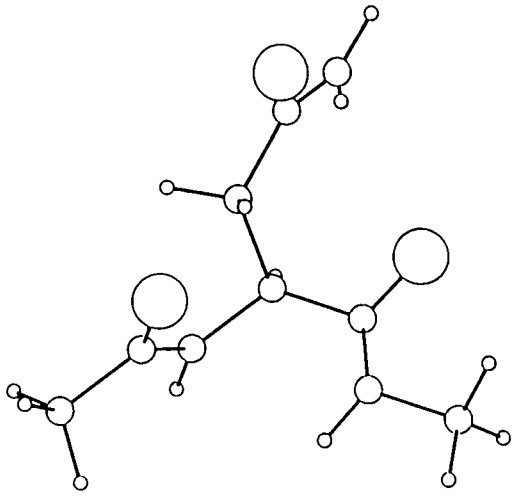

Fig. 1. Dipeptide model used for reference free energy calculations, shown with an Asn side chain.

for simulations of the antibody–antigen complex, but similar procedures were used for the unliganded antibody and for reference simulations of dipeptide molecules, except where otherwise noted.

The force-field used in all the simulations is that of the CHARMM program (Brooks *et al.*, 1983), version 20. An extended-atom approach was taken for most carbon atoms bearing non-polar hydrogen atoms. The all-atom representation was used only for the side chain of Asn (Asp)31^L. In that side chain, χ^1 is effectively confined by steric repulsion with the neighboring peptide groups in their main chain conformation, so that the principle degree of freedom is χ^2 (see Figure 1). In the free energy perturbation calculations, the torsional energy potential for χ^2 was replaced by a harmonic potential which was fitted to the gauche torsional energy well corresponding to the crystallographic conformation and restrained the sampling to that well. In free energy perturbations of the side chain, a restrained conformation avoids the need for longer sampling that may arise from the conformational isomerization of the mutating groups.

The mass of all explicit H atoms was weighted by a factor of 10 so as to restrict the high-frequency vibration of covalent bonds involving hydrogens, which allowed the use of a time step increased to 4 fs (Pomès and McCammon, 1990). The Verlet algorithm was used to propagate the equations of motion. All non-bonded energy calculations were truncated, at 8 Å with a switching function in the case of van der Waals interactions and at 8.5 Å with a shifting function in the case of Coulombic terms.

Because of the extended size of the system, a 'solvated droplet' model (Shen *et al.*, 1989) was set up. A sphere 26 Å in radius was selected, centered on C_γ of Asn31^L of the antibody. This sphere includes all four loops of the L chain, all three CDR loops of the H chain of the antibody and most of the antigen. Residues lying entirely beyond the 26 Å boundary from the center were deleted. As described below, a spherical droplet of TIP3P water molecules (Jorgensen *et al.*, 1983) was used to solvate the protein system. During all subsequent dynamical stages, only those residues lying within 15 Å of the droplet center were allowed to move.

No positional restraints were applied to atoms inside the dynamical system in the simulations of the complex, but a

weak harmonic restraint was used on the C_γ of Asn31 (Asp in the mutant) in the dipeptide simulations, so as to keep the small solute at the center of the droplet. The simulations of the unliganded antibody were run twice, once with no restraints and once with harmonic restraints on the backbone dihedral angles of the loops of the L chain, in an attempt to gauge the influence of backbone conformational flexibility and to facilitate the comparison of molecular dynamics results with the outcome of Poisson–Boltzmann calculations, performed in the assumption of fixed geometry. The latter antibody system is henceforth referred to as 'conformationally restrained Fab'.

Some care was taken in order to ensure realistic protonation states of histidine side chains. The orientation and protonation site of each of the buried His rings were assessed using molecular mechanics energy calculations so as to identify the combination leading to the best hydrogen bonding with neighboring residues.

Solvation procedure

A large sphere of TIP3P waters (Jorgensen *et al.*, 1983) equilibrated at 300 K was superimposed on the protein model. Solvent molecules whose oxygen centers lay within 2.4 Å of any protein heavy atom were deleted. This procedure left a number of waters either buried in the protein interior or trapped at the interface between the H, L, and HEL chains, molecules whose fate was decided according to the following criteria. Molecular mechanics calculations were performed for a water probe placed successively on the points of a grid overlapping the unsolvated protein complex, using the program GRID (Goodford, 1985; Boobbyer *et al.*, 1989). Isoenergetic contours were then calculated and displayed at hydrogen bonding energy levels (typically, below −8.0 kcal/mol) in order to identify potentially solvated cavities. TIP3P molecules were then placed into these contours, oriented so as to minimize the hydrogen bonding energy, and subjected to short energy minimizations while the protein heavy atoms were held fixed. CHARMM molecular mechanics energies were then calculated individually for these buried solvent molecules and their values compared to the previously obtained GRID values. Only those water molecules participating in strong hydrogen bonds with surrounding residues were retained. This procedure was made necessary by the discrepancies between GRID and CHARMM energies and its difficulty was compounded by the concurrent need to reassess the protonation states of nearby histidine side chains and by the possibility of water–water interactions within cavities or channels. The ultimate test of assessing cavity solvation was provided during thermalization of the solvent, when a buried water molecule diffused through the protein interior and was subsequently deleted.

Equilibration

Before proceeding with molecular dynamics, a number of steps were required to ensure the removal of bad contacts between atoms and the orientational relaxation of water molecules at the interface with the protein(s). This is achieved through successive energy minimizations and dynamical thermalization of the solvent and the protein residues of the inner sphere. The algorithm chosen for these minimizations uses the steepest descent procedure so as to leave the system in a local minimum close to the crystallographic conformation. For the same reason, the solvent is thermalized first, before the heavy atoms of the protein are allowed to move.

First, the hydrogen atoms of water molecules inside the 19 Å boundary were subjected to 100 steps of minimization, during which the protein atoms were fixed and the positions of water oxygen atoms were restrained via a steep harmonic potential. The energy of water molecules inside the 15 Å boundary was then refined with 200 steps of minimization, after which the solvent within that inner dynamical sphere was thermalized in the following fashion: three stages of 2 ps simulations with temperature gradients followed by 3 ps equilibrations, at 100, 200 and 300 K successively. The solvent was then taken through 5 ps of equilibration with velocity reassignments at 300 K every 0.2 ps. At that stage, an ultimate comparison of surface and buried water locations with the low-energy contours constructed using GRID proved satisfactory, which provided confidence in the solvation of the crystallographic structure.

The positions of solvent molecules were then fixed and the protein residues inside the dynamical sphere were taken through 200 steps of steepest-descent energy minimization. The procedure followed to thermalize the protein ran over 18 ps and mirrored that used for the solvent.

All residues inside the dynamical sphere were then allowed to move and the system was subjected to a 10 ps equilibration with velocity reassignments every 0.2 ps, followed by 10 ps with velocity reassignments every picosecond. Equilibration was then completed with a 20 ps run with temperature relaxation. Small r.m.s. deviations of the positions of inner atoms confirmed the stability of the structure and the convergence of the equilibration.

Free energy calculations

Free energy differences were calculated using the perturbation algorithm of CHARMM. The perturbations were made on a hybrid side chain with a unique topology up to and including C_γ and both Asn and Asp terminal atoms present (dual topology). Consistent with the topology and parameters of the CHARMM force-field, the types and parameters of all atoms besides the terminal NH_2 and O atoms of the Asn and Asp side chains were identical during the simulation, except for the partial charges attributed to C_γ and to C_β and its H substituents, which varied with λ during the perturbation.

An initial perturbation run using the double sampling technique (Beveridge and Dicapua, 1989) with five reference points at respectively λ = 0.1, 0.3, . . ., 0.9 was performed on the dipeptide system and yielded a free energy profile characteristic of a charge creation in aqueous solution. In order to limit the free energy difference of each integration step to the order of thermal fluctuations (kT) and thus reduce sampling problems (McCammon and Harvey, 1987), all subsequent mutations were broken down into 77 integration steps with λ spacings of 0.01 between 0.01 and 0.05 and between 0.49 and 0.99 and spacing of 0.02 between 0.05 and 0.49. At each integration step, a minimum of 2 ps of equilibration with velocity reassignments every 0.2 ps and a minimum of 2 ps of data collection were run. During the production stage, coordinate sets and the energy values of the reference and perturbed states were stored every 0.02 ps for post-processing. In the case of the complex, an additional 2 ps of production was run at each integration step so as to help assess convergence. The total length of each perturbation thus ranged between 336 and 452 ps.

Data were then analyzed using the CHARMM algorithm with both the integration and the perturbation methods. A minimum of 42 500 configurations was used to compute each overall free energy change, but 20 times fewer configurations were used for the decomposition.

Poisson–Boltzmann calculations

The electrostatic energy contributions to the difference in the solvation energy of the Asn and Asp dipeptides and to the relative free energy of binding of wild type and mutant HyHEL-10 with HEL were estimated by means of continuum electrostatic calculations using the finite difference Poisson–Boltzmann (PB) algorithm of the University of Houston Brownian Dynamics (UHBD) program (Davis *et al.*, 1991). The theory and methodology of such calculations is described elsewhere (Gilson *et al.*, 1987).

The conformations used for the PB calculations were obtained as averages from 20 ps molecular dynamics trajectories of the Asn and Asp dipeptides and of the wild type and mutant Fab–Ag complexes, after energy minimization of the positions of hydrogen atoms. The solvation energy of the dipeptides was calculated as the difference between electrostatic energies of the solute in a continuum with dielectric constants of 1 and 78, successively. The electrostatic binding energy of the complex was calculated as the difference between the electrostatic energy of the Fab–Ag complex and its analogs for the isolated Fab and Ag moieties in a solvent continuum with dielectric constant 78. In these calculations, the conformation of the Fab and Ag moieties was assumed to be retained upon decomplexation. The entire antigen-binding fragment of the antibody, Fab, was included. The charges used were identical to the CHARMM set used in the MD simulations. The N- and C-termini were assumed to be charged. No buried water molecule was included. All protonation states and partial charges were consistent with those used in the MD simulations. The ionic strength was set to zero; the solute dielectric was taken to be 4. A grid size of 65^3 with a spacing between grid points of 0.3 Å was found to be adequate in the finite-difference calculations of the dipeptide system. In the finite-difference calculations of the complex system, a grid of $90\times90\times110$ with a spacing of 1.0 Å was used as a starting point so as to include the entire Fab–Ag complex. Focusing was then used; the focusing grid was made large enough to include the dynamical MD system and contained 105^3 points with a spacing of 0.5 Å. Calculations were performed on the same focusing grid so that the self-energy terms would cancel for each binding energy moiety of the cycle (see equation 1). Tests of convergence of the PB calculations included varying the size of the grid by ±1 unit and varying the grid spacing by $\pm10\%$ of its value.

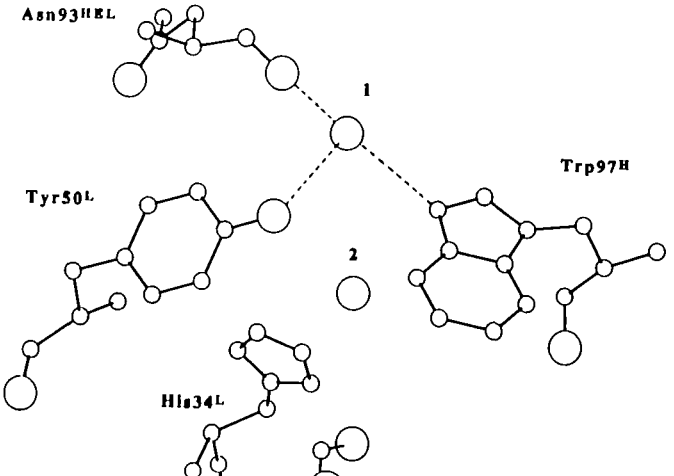

Fig. 2. Cross-section of a hydrated channel at the core of the Fab–Ag complex obtained from a 20 ps averaged trajectory showing two water molecules labeled 1 and 2. The hydrogen bonds involving water 1 are shown as dashed lines. They bridge all three polypeptide chains H, L and HEL together.

Results

Solvation

The procedure used for solvation led to the hydration of six cavities and, importantly, of a channel extending from the

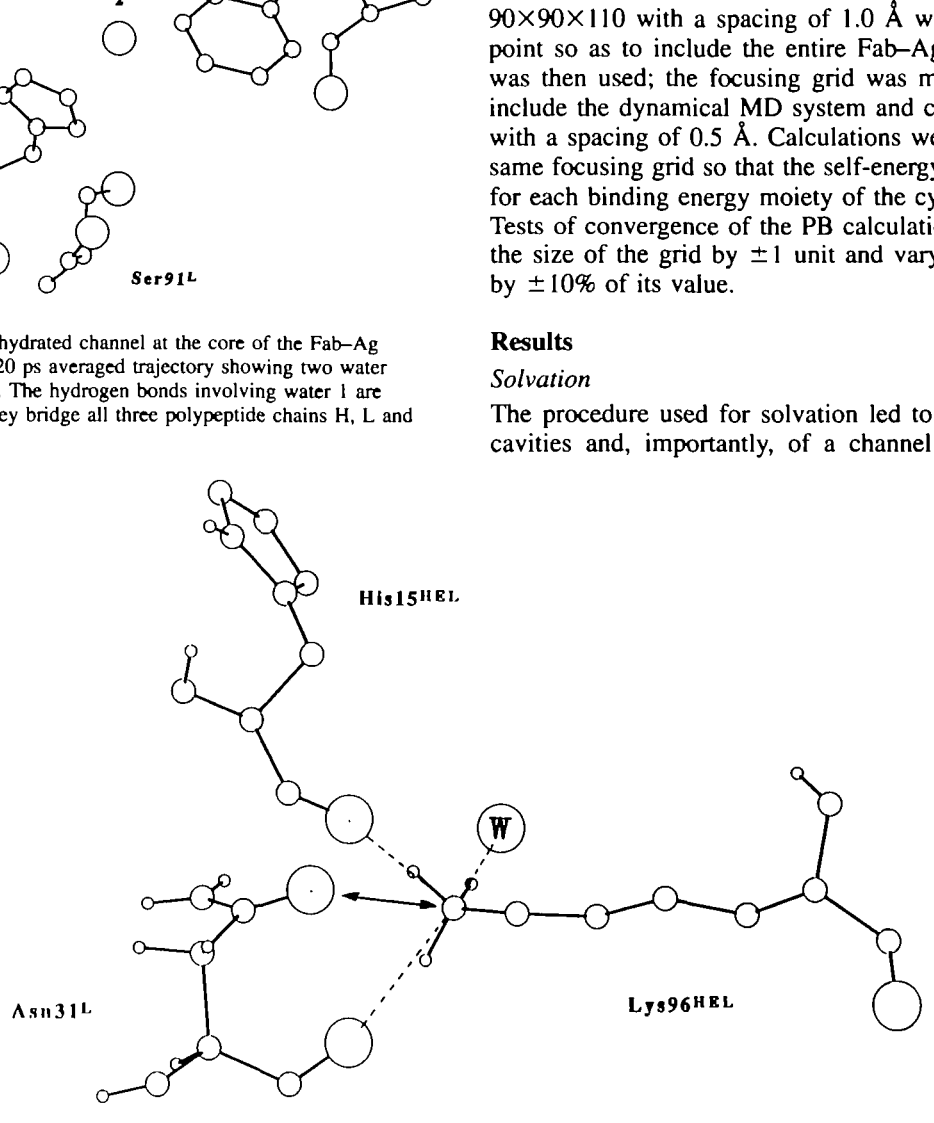

Fig. 3. Cross-section of the Asn31^L–Lys96^{HEL} region of the Fab–Ag interface obtained from a 20 ps averaged trajectory showing the proximity of a (buried) water molecule. The hydrogen bonds involving the positively charged lysine terminal are shown in dashed lines, while the double arrow indicates the salt link to be created with Asn to Asp mutation of residue 31^L.

edge of the antibody–antigen interface into the core of the assembly between the L and H chains on the one hand and HEL on the other. This channel was found to accommodate three water molecules, two of which are depicted in Figure 2 with a few surrounding residues.

One of the water molecules solvating this channel forms hydrogen bonds between all three of the polypeptide macromolecules. Such hydration sites appear of structural importance to the quaternary assembly since (i) they help conserve the crystallographic conformation of channel residues around them and (ii) their hydrogen bond network is well conserved over molecular dynamics trajectories extending into the hundreds of picoseconds.

Another hydrated pocket, in contact with the terminal of $Lys96^{HEL}$, was found to accommodate one water molecule that makes a very stable hydrogen bond with the charged NH_3 donor, as depicted in Figure 3. The presence of this water molecule is important because it could compete with the formation of the proposed salt link between $Lys96^{HEL}$ and $Asp31^{L}$. In addition to the procedure described previously, short simulations run with and without that water molecule showed that it helps preserve the local crystallographic conformation around the $Lys96^{HEL}$ terminal (see Figure 3).

Antibody conformational flexibility

The backbone torsional angles of the loops of the L chain of the antibody were calculated as averages from 20 ps molecular dynamics trajectories computed at all four points of the thermodynamic cycle (see equation 1) and are listed in Table I. In this table, the names of residues making up the loop turns proper appear in bold face and significantly large values or changes are stressed with bold face type. The organization of

Table I. Main chain dihedral angles (ϕ, ψ) of residues making up the loops of the antibody L chain calculated respectively from the crystallographic coordinates and the dynamical averages for the wild type (wt) and mutant (mu) proteins, successively for the complexed and uncomplexed systems Fab–Ag and Fab

Loop	Residue	X-ray		Fab–Ag				Fab			
		wt		wt		mu		wt		mu	
CDR_1	Cys23	−155,	107	−159,	97	−160,	96	−161,	107	−133,	**155**
	Arg24	−104,	109	−91,	135	−90,	137	−99,	127	**−142,**	134
	Ala25	−85,	135	−81,	177	−80,	176	−80,	164	−96,	177
	Ser26	−88,	64	−88,	64	−88,	64	−99,	15	−59,	**−68**
	Gln27	172,	160	−157,	175	−149,	158	−150,	167	**−104,**	170
	Ser28	−64,	−38	−99,	**93**	−80,	**99**	−60,	−46	−75,	−7
	Ile29	9,	63	**−129,**	62	**−132,**	**160**	34,	47	47,	29
	Gly30	−63,	107	−63,	146	**−146,**	156	−37,	106	**60,**	**23**
	Asn31	85,	−15	**43,**	**49**	**36,**	**59**	**47,**	**48**	**54,**	**41**
	Asn32	−105,	72	−129,	**6**	−158,	38	−132,	51	−109,	73
	Leu33	−129,	119	−111,	148	−123,	145	−120,	146	−127,	143
	His34	−126,	145	−123,	155	−118,	148	−122,	160	−130,	164
	Trp35	−104,	138	−121,	143	−116,	140	−127,	144	−126,	145
	Tyr36	−125,	172	−128,	152	−127	151	−129,	153	−128,	154
CDR_2	Leu46	−81,	138	−76,	145	−77,	148	−71,	140	−72,	143
	Leu47	−104,	−66	−113,	−73	−116,	−81	−112,	−73	−116,	−70
	Ile48	−121,	133	−119,	145	−110,	142	−119,	139	−122,	137
	Lys49	−92,	179	**−119,**	148	**−116,**	150	**−116,**	155	**−110,**	155
	Tyr50	30,	−72	73,	−52	70,	−61	47,	**36**	47,	**43**
	Ala51	−158,	−41	−177,	−41	−165,	−43	**60,**	−11	**60,**	−10
	Ser52	−134,	7	−142,	1	−135,	−14	−139,	−22	−141,	−35
	Gln53	−86,	102	−77,	104	−73,	122	−84,	147	−76,	139
	Ser54	−73,	134	−71,	115	−79,	151	−94,	148	−84,	145
	Ile55	−70,	167	−71,	−177	−97,	−176	−77,	173	−75,	173
	Ser56	−97,	136	−110,	136	−53,	135	−97,	136	−97,	136
Non-CDR	Phe62	−80,	135	−80,	135	−92,	144	−80,	135	−83,	134
	Ser63	−149,	141	−152,	150	−156,	162	−152,	151	−150,	161
	Gly64	−137,	155	−136,	165	−156,	170	**−104,**	155	−125,	149
	Ser65	−161,	175	−144,	169	−151,	164	−147,	180	−137,	164
	Gly66	108,	177	**156,**	137	**168,**	124	99,	147	**146,**	169
	Ser67	163,	141	−153,	150	−156,	164	−144,	**−33**	−142,	**−12**
	Gly68	113,	−122	62,	−100	80,	−85	**−87,**	**−144**	**−149,**	**−136**
	Thr69	−105,	−48	−118,	−18	−144,	−39	**−79,**	−9	**−73,**	−17
	Asp70	−75,	112	**−111,**	132	**−103,**	136	**−104,**	137	**−101,**	142
	Phe71	−129,	134	−130,	149	−121,	150	−127	159	−132,	151
	Thr72	−140,	151	−140,	157	−140,	148	−140,	160	−135,	141
	Leu73	−127,	123	−134,	149	−125,	146	−135,	142	−116,	134
	Ser74	−113,	135	−134,	139	−129,	140	−125,	141	−128,	133
CDR_3	Phe87	−115,	166	−126,	156	−120,	141	−118,	158	−100,	131
	Cys88	−124,	161	−114,	156	−105,	155	−112,	155	−82,	150
	Gln89	−152,	126	−144,	156	−143,	150	−137,	145	−142,	144
	Gln90	−92,	166	−107,	145	−120,	143	−107,	136	−105,	146
	Ser91	−145,	16	−110,	10	−111,	3	−112,	20	−130,	29
	Asn92	−72,	−48	−85,	−74	−88,	−67	−93,	−58	−97,	−46
	Ser93	−126,	153	−88,	148	−95,	153	−113,	147	−121,	150

The names of residues making up loop turns appear in bold face type, as do the values of dihedral angles that deviate largely from the crystallographic reference or from each other. All values are in degrees.

Table I follows the secondary structure of the L chain's antigen-binding region, with four loop turns labeled CDR_1 to CDR_3 and 'non-CDR' connecting strands of β-sheet. The residues making up the β-sheet structure have (ϕ, ψ) main-chain angles in the vicinity of (−120, 140), whereas the torsions in the residues making up the turns, whose length and conformations vary, depart from these values. The list of residues in Table I nearly matches that of these antibody residues that are within the dynamical sphere; thus, the H chain is excluded and the L chain's CDR_3 turn is truncated whereas all other three loop turns figure in the vicinity of the site of mutation and are entirely included. The β-sheet structure is conserved in all four systems, as most main chain conformational reorientations take place in loop turns, particularly CDR_1 and the non-CDR loop. Most of the transitions go in pairs that involve the ψ angle of a residue and the ϕ angle of the following residue, such as residues 23–24, 26–27, 28–29, 29–30, 50–51, 67–68 and 68–69. The wild type and mutant Fab–Ag complexes display main chain conformations consistent with each other (with the exception of the peptide bond linking residues 29 and 30) and, to a lesser extent, consistent with the crystallographic structure (see residues 28–29, 31 and 66). The change in the conformation of residue 31^L of CDR_1 in the Fab–Ag systems with respect to the crystallographic structure is due to the formation of a very stable hydrogen bond between the main chain carbonyl of that residue and the terminal of $Lys96^{HEL}$, as shown in Figure 3, and does not extend to the uncomplexed Fab systems. On the other hand, the uncomplexed, wild type antibody's main chain conformation departs from the crystallographic folding in loop CDR_2 (residues 50 and 51) and in the non-CDR loop (residues 67–69). These reorientations extend to the mutant Fab case and appear to be a direct consequence of solvating the hypervariable region of the antibody after removal of the antigen. The mutant Fab also

Table II. Antibody L chain C_α deviations between dynamical averages and the crystallographic structure (bold face type) and r.m.s. fluctuations in the wild type (wt) and mutant (mu) proteins, successively for the complexed and uncomplexed systems Fab–Ag and Fab

Loop	Residue	Fab–Ag				Fab			
		wt		mu		wt		mu	
CDR_1	Cys23	**0.20**	0.14	**0.31**	0.09	**0.30**	0.13	**1.05**	0.13
	Arg24	**0.63**	0.19	**0.69**	0.00	**0.40**	0.20	**0.67**	0.18
	Ala25	**0.43**	0.16	**0.50**	0.12	**0.39**	0.17	**0.30**	0.14
	Ser26	**0.00**	0.00	**0.16**	0.00	**0.30**	0.00	**1.30**	0.00
	Gln27	**0.32**	0.15	**0.37**	0.15	**0.32**	0.14	**1.17**	0.15
	Ser28	**0.36**	0.26	**1.06**	0.19	**0.25**	0.28	**1.79**	0.27
	Ile29	**0.80**	0.31	**2.16**	0.30	**0.30**	0.31	**0.71**	0.34
	Gly30	**0.90**	0.34	**1.57**	*0.40*	**0.71**	*0.47*	**2.34**	0.34
	Asn31	**0.81**	0.25	**1.18**	0.24	**0.49**	*0.40*	**1.11**	0.30
	Asn32	**0.62**	0.27	**0.33**	0.34	**0.63**	0.36	**0.51**	0.30
	Leu33	**0.72**	0.28	**0.77**	0.29	**0.50**	*0.40*	**0.47**	0.31
	His34	**0.45**	0.31	**0.80**	0.29	**0.39**	0.24	**0.10**	0.28
	Trp35	**0.22**	0.24	**0.31**	0.24	**0.28**	0.19	**0.16**	0.26
	Tyr36	**0.35**	0.18	**0.34**	0.17	**0.37**	0.15	**0.30**	0.18
CDR_2	Leu46	**0.08**	0.15	**0.03**	0.13	**0.13**	0.13	**0.12**	0.15
	Leu47	**0.23**	0.23	**0.17**	0.20	**0.39**	0.25	**0.25**	0.24
	Ile48	**0.33**	0.29	**0.43**	0.27	**0.69**	0.26	**0.55**	0.30
	Lys49	**0.54**	0.34	**0.57**	0.30	**0.71**	0.29	**0.81**	0.35
	Tyr50	**0.50**	0.31	**0.53**	0.29	**0.54**	0.38	**1.20**	0.34
	Ala51	**0.49**	0.33	**0.56**	*0.40*	**0.95**	*0.49*	**1.11**	0.35
	Ser52	**0.15**	0.31	**0.24**	0.32	**0.72**	*0.44*	**0.65**	0.34
	Gln53	**0.19**	0.32	**0.53**	0.29	**0.54**	0.29	**1.15**	0.29
	Ser54	**0.39**	0.33	**0.51**	0.26	**0.10**	0.28	**0.41**	0.26
	Ile55	**0.62**	0.22	**0.94**	0.16	**0.00**	0.15	**0.12**	0.17
	Ser56	**0.00**	0.00	**0.86**	0.00	**0.00**	0.00	**0.00**	0.00
Non-CDR	Phe62	**0.00**	0.00	**0.16**	0.00	**0.00**	0.00	**0.21**	0.00
	Ser63	**0.25**	0.14	**0.50**	0.15	**0.32**	0.15	**0.27**	0.13
	Gly64	**0.18**	0.33	**0.47**	0.39	**0.26**	0.35	**0.63**	0.13
	Ser65	**0.63**	0.33	**0.45**	0.37	**1.66**	0.31	**1.95**	0.31
	Gly66	**1.25**	*0.53*	**1.46**	0.35	**1.93**	0.36	**2.07**	0.28
	Ser67	**1.19**	*0.45*	**1.05**	0.27	**2.94**	*0.44*	**4.28**	0.29
	Gly68	**0.69**	0.35	**1.41**	0.28	**2.85**	*0.50*	**2.43**	0.32
	Thr69	**0.75**	0.36	**0.59**	0.20	**0.54**	0.38	**0.66**	0.20
	Asp70	**0.90**	0.33	**0.72**	0.23	**1.04**	0.35	**0.59**	0.19
	Phe71	**0.45**	0.28	**0.33**	0.23	**0.14**	0.28	**0.39**	0.21
	Thr72	**0.29**	0.27	**0.10**	0.23	**0.16**	0.23	**0.52**	0.20
	Leu73	**0.26**	0.24	**0.22**	0.18	**0.26**	0.29	**0.42**	0.15
	Ser74	**0.25**	0.15	**0.28**	0.13	**0.08**	0.18	**0.11**	0.00
CDR_3	Phe87	**0.12**	0.00	**0.29**	0.00	**0.00**	0.00	**0.20**	0.00
	Cys88	**0.11**	0.14	**0.10**	0.13	**0.16**	0.13	**0.75**	0.14
	Gln89	**0.07**	0.19	**0.18**	0.18	**0.13**	0.20	**0.62**	0.22
	Gln90	**0.44**	0.25	**0.13**	0.25	**0.24**	0.22	**0.42**	0.27
	Ser91	**0.60**	0.28	**0.79**	0.38	**0.72**	0.25	**0.68**	0.29
	Asn92	**1.00**	0.25	**0.70**	0.26	**0.53**	0.23	**0.52**	0.26
	Ser93	**0.30**	0.19	**0.31**	0.19	**0.11**	0.19	**0.20**	0.18

All values are in angstroms. The names of residues making up loop turns proper appear in bold face type. R.m.s. fluctuations >0.4 Å are in italic.

displays further changes in the conformation of its CDR_1 (see residues 23–24, 26–27 and 30). More detailed observations are needed in order to assess whether these further changes are directly induced by the mutation or whether they simply result from additional sampling, some 400 ps down the dynamics trajectory.

The C_α deviations from the crystallographic conformation, and the r.m.s. fluctuations of individual C_αs are listed in Table II. These data illustrate the nature of the limited structural changes taking place upon mutation and/or upon desolvation of the antigen binding surface and are consistent with the peptide reorientations evidenced in Table I. In fact, all the C_α displacements in excess of 1.0 Å and most of the large r.m.s. fluctuations of the C_α atoms (upwards of 0.40 Å) occur at or next to residues whose backbone underwent conformational reorientation with respect to the crystallographic fold. In particular, the CDR_1 residues of mutant Fab–Ag and Fab systems affected by backbone transitions display large displacements and record displacements of up to 4 Å are reached in the Fab cases by non-CDR loop residues that have unfolded into the solvent. Larger r.m.s. fluctuations generally occur in both of the wild type Fab–Ag and Fab systems compared to their mutant counterparts, but this is more obvious in the unliganded Fab case, suggesting that in spite of the screening of Coulombic interactions by the high dielectric solvent, the aspartate charge introduced upon the Asn to Asp mutation might assist in restricting the mobility of nearby residues' backbone dipoles, particularly Gly30, Asn31, Ala51, Ser52, Ser67 and Gly68. To some extent, however, the enhanced mobility of the wild type Fab may also result from incomplete equilibration. In the following analysis, we try to address these questions in more detail.

Binding free energy

The overall free energy changes for the Asn to Asp mutations in the dipeptide, complex and unliganded Fab systems are given in Table III. The relative solvation free energy of the dipeptides, before electrostatic cut-off correction, is −54.9 kcal/mol (second column in the table). The relative binding free energy of the mutant antibody is −5.6 kcal/mol (columns 3 and 4). The calculation performed with harmonic restraints on the unliganded antibody's main chain conformation (columns 3–5), is also included in Table III for later comparison with continuum electrostatic calculations. There is no straightforward way to estimate the statistical error attached to these values, but a number of alternative calculations using fewer perturbation steps, a different number of configurations, extended sampling collection and different algorithms for the calculation may help in assessing the convergence of the results. The values obtained for the dipeptide mutation using the perturbation method with five steps and the integration method with 77 steps are respectively −54.1 and −54.9 kcal/mol, within 2% of each other. One expects the calculation with fewer integration steps to be subject to somewhat larger statistical errors because the changes in free energy between successive steps may be large compared to thermal fluctuations, thus making the reference ensemble unrepresentative of the perturbed one, which in turn leads to larger statistical uncertainty. On the other hand, the values obtained using the perturbation method should be the same as those obtained from the same trajectory with the thermodynamic integration method in the limit of infinite sampling. In our simulations, they are separated by 0.2 and 0.1% respectively in the Fab–Ag complex and the free, unliganded Fab cases. These errors are small and concentrated at the end-points. Calculating the free energy difference for the mutation in the Fab–Ag complex using 20-fold fewer configurations and 50% more (from additional sampling) yielded free energy differences of −52.8 and −52.2 kcal/mol respectively. These values lay respectively within 0.6 and 0.1 kcal/mol from the value obtained with the standard procedure described in the Materials and methods section. Thus, the convergence of the free energy value seems within reasonable reach of our simulations. The values retained for the calculation of the relative free energy of binding of the mutant antibody were chosen as the average of the values obtained respectively with the perturbation and the thermodynamic integration (equations 2 and 4). This yields a relative binding free energy change of −5.6 kcal/mol for the flexible chain antibody and −0.5 kcal/mol in the case where the unliganded antibody's main chain conformation is restricted.

Other sources of statistical error due to conformational sampling include possibly insufficiently sampled conformations of the flexible antigen-binding antibody loops and the sampling of the mutating side chains' conformations. The former constitutes a potentially formidable problem, because the time scale corresponding to loop conformational rearrangements may extend into the thousands of picoseconds, a time range not easily accessible with current molecular dynamics of biomacromolecules. Among the other degrees of freedom of the antibody molecule that may be restricted upon antigen binding are those defining the torsional isomers of the mutating side chain itself. Unless the native and mutant side chains have identical rotamers and identical equilibrium distributions of rotameric states (which is unlikely), a contribution to the free energy will arise from substituting one side chain for the other (Straatsma and McCammon, 1989). This contribution was estimated elsewhere using potential of mean force calculations on solvated Asn and Asp dipeptide systems (Pomès, 1993) and was found to be small (–0.2 kcal/mol) compared with the overall free energy change for the Asn to Asp mutation reported in the present study. This justifies the neglect of secondary rotamers of the mutating side chain imposed by the

Table III. Helmholtz free energy changes for $Asn31^L$ to Asp mutation in a dipeptide model, the HyHEL-10–HEL complex, the unliganded HyHEL-10 antibody, the conformationally restricted HyHEL-10 antibody (see text) and the thermodynamic-cycle perturbation values for columns 3 and 4 and for 3–5 respectively

	Dipeptide	Fab–Ag	Fab	Fab*	Columns 3 and 4 cycle	Columns 3 and 5 cycle[a]
Total	–54.9	–52.2	–46.5	–51.7	–5.6	–0 5
Van der Waals	–2.2	–3.4	–2.3	–2.1	–1.1	–1.3
Electrostatic	–47.7	–40.7	–36.8	–41.8	–3 8	1 2
Covalent	–4.5	–8.6	–7 1	–7.0	–1 5	–1.5

All values are in kcal/mol.
[a]Conformationally restrained antibody backbone.

harmonic potential on χ^2 in the free energy calculations reported here.

The systematic error due to insufficient equilibration of the system can be estimated by calculating free energy differences using two different sets of energy values: (i) those collected immediately after equilibration (0–2 ps) and (ii) those obtained from additional sampling (2–4 ps) at every integration step. These values were calculated for the Fab–Ag perturbation calculation as −52.22 and −52.29 kcal/mol, respectively. The relative error between these two amounts to less than 0.2%, well within the statistical error. We therefore consider the extent of equilibration sufficient in all the calculations reported here.

Other systematic errors include those arising from the force-field and the truncation of non-bonded interactions. The comparison of results obtained from our reference calculations on dipeptide molecules with experimental data provides an approximate measure of the model's performance in those respects. The experimental value of the difference in the free energy of hydration of acetate with respect to acetamide is directly deduced from reported data (Pearson, 1986) as −73 ± 2 kcal/mol. This compares fairly well to our calculated value of −75 kcal/mol for the relative hydration free energy of an aspartate versus an asparagine dipeptide. The latter value was obtained from the 77-step perturbation run, after correcting for the truncation of long-range electrostatic interactions with the Asp charge. This correction was approximated by subtraction of the Born free energy for solvating a singly-charged 8.5 Å radius spherical cavity into a continuum with a dielectric constant of 78.5 (Born, 1920; Straatsma and Berendsen, 1988). The Born correction amounts to −20.5 kcal/mol, which brings our calculated Asn to Asp dipeptide relative solvation free energy value from −54.9 to −75.4 kcal/mol. Consistently, the relative solvation free energy of the Asp dipeptide with respect to Asn obtained from continuum calculations with the finite-difference Poisson–Boltzmann method was found to be −76 kcal/mol. These results seem to indicate that the force-field is reasonably adequate for the calculation and that the Born correction provides a crude but fair approximation of the truncated solvent–solute interactions.

In cases where protein residues extend beyond the cut-off distance from the new charge, however, the uncertainty due to the cut-off distance of long-range interactions constitutes an outstanding problem because the Born approximation cannot be applied. This is the case of all four stages of the thermodynamic cycle for Fab and Fab–Ag, where both antigen and antibody proteins extend well beyond the cut-off radius. In our protein free energy simulations, we note that the only full charges within the cut-off from the center of charge of the mutating residue are those of Lys96 in the antigen and $Asp31^L$ itself. The free energy perturbations, therefore, involve consistent changes in the net charge within the cut-off, respectively from 0 to −1 (unliganded Fab) and from +1 to 0 (Fab–Ag complex). Although in principle the Poisson–Boltzmann calculations might be preferred over the free energy simulations because they take into account the long-range component of the electrostatic energy, the large error that would result from the imbalance of charges within the cut-off was avoided in the present simulations.

In the future, the long-range component of the electrostatic contribution could be estimated separately using continuum techniques more sophisticated than the Born model for solvation, such as those utilizing the Poisson–Boltzmann equation to calculate the electrostatic field on a grid superimposed on the solute(s) via finite-difference approximations (Warwicker and Watson, 1982; Davis and McCammon, 1989). This is a challenging problem, especially because of the rapidly changing state of the PB art (Antosiewicz *et al.*, 1994).

Decomposition of the free energy change

Overall physical contributions. The free energy results were broken down approximately into different overall physical contributions: internal (bonded), non-bonded electrostatic and non-bonded van der Waals. These results are shown in Table III.

The electrostatic term dominates and contributes ~80% to the free energy change for the mutation in all three systems. Whereas both protein mutations yield an electrostatic term less negative than their 'fully solvated' dipeptide counterpart, the value for Fab–Ag is smaller than that of Fab alone, which suggests that the penalty for burying a charge is more than made up for by the salt link introduced by pairing the charges of $Asp31^L$ and $Lys96^{HEL}$. However, this does not hold in the case of the conformationally restrained unliganded antibody (column 4 in Table III), for which the electrostatic term is more comparable to that of the complex. Accordingly, the relative electrostatic binding free energy of the mutant Fab calculated with the Poisson–Boltzmann method was found to be 1.8 kcal/mol, in fair agreement with the molecular dynamics free energy calculation result of 1.2 kcal/mol for the restrained-Fab cycle. In the Poisson–Boltzmann calculations, the Fab and Ag moieties retain their crystallographic conformations and the agreement suggests that the electrostatic cut-off correction to the molecular dynamics simulation results is likely to be small for this system. The PB calculations also confirm that with the assumption of a rigid Fab backbone, the single-point mutation is unfavorable in electrostatic terms. However, the favorable value of −3.8 kcal/mol obtained for the cycle in which no restriction was imposed on the backbone of the unliganded Fab indicates that assuming conservation of the Fab loops conformation upon solvation or desolvation, as the lock and key mechanism would imply, may not be valid in this case.

The van der Waals contribution is small in all cases, which reflects the isosteric nature of the mutation. Thus, the analysis

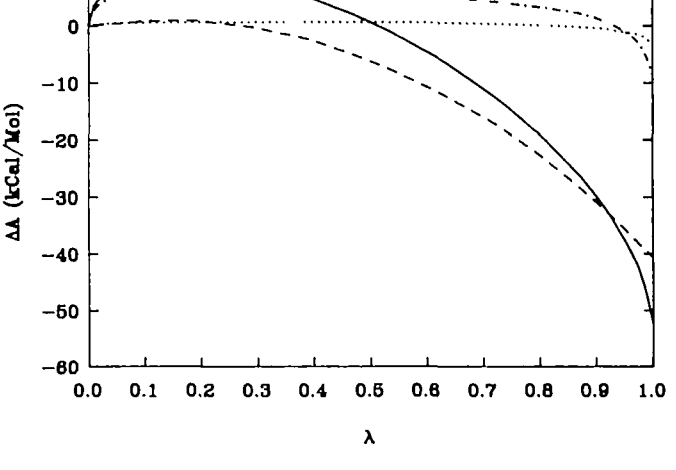

Fig. 4. Helmholtz free energy change for Asn (λ = 0) to Asp (λ = 1) mutation of residue 31^L in the Fab–Ag complex, as a function of the perturbation parameter λ, is indicated by a solid line. Its components are also shown as follows: dashed for electrostatic, dash–dotted for covalent and dotted for Lennard–Jones.

of non-bonded interactions will undoubtedly be accounted for in terms of interactions involving polar and charged groups.

The covalent term, on the other hand, contributes significantly to the mutation free energies in the protein systems. Because this term is a measure of the internal stress applied on the mutating side chain, it is interesting to relate it to the path followed by the mutation. Figures 4 and 5 depict the change in free energy as a function of the perturbation parameter respectively in the liganded and unliganded antibody cases. In these plots, the left-hand side corresponds to the Asn case, whereas $\lambda = 1$ corresponds to the Asp side chain. The plots of the covalent contribution show strong slopes at the end-points but are almost level in between. This reflects the stress introduced in the systems as dummy atoms are created (at early stages of the simulation) and deleted (at late stages). Because these appearing and vanishing atoms contribute only a fraction of their full potential, their mobility is increased and some instability results in the integration of the equations of motion. Methods have been developed to circumvent that problem, but they have their own shortcomings. One approach consists of constraining the location of the 'dummy' atoms to that of their full-atom mutant or wild type counterpart, but this could impair the relaxation of nearby polar groups and solvent molecules during the conversion of NH_2, a hydrogen bond donor, into O, a hydrogen bond acceptor. Another method, used more commonly for non-isosteric perturbations, consists of growing or decreasing the bond-length parameters, as well as the van der Waals radius, of the appearing or disappearing particles during the perturbation. This is the so-called 'sprouting' and 'desprouting' technique. It has been pointed out (Pearlman and Kollman, 1991; Straatsma *et al.*, 1992) that such methodology is valid only if side studies are carried out to assess constraint contributions to the free energy difference otherwise unaccounted for by the method. In this study, no holonomic constraint linking the mutating groups was imposed. Instead, each of the dihedral potential terms governing the χ^2 torsion of Asn and Asp terminal groups was replaced by a harmonic well so as to prevent their full rotation and the approach taken simply allowed extra sampling at the end-points. Because the covalent contribution to the free energy is

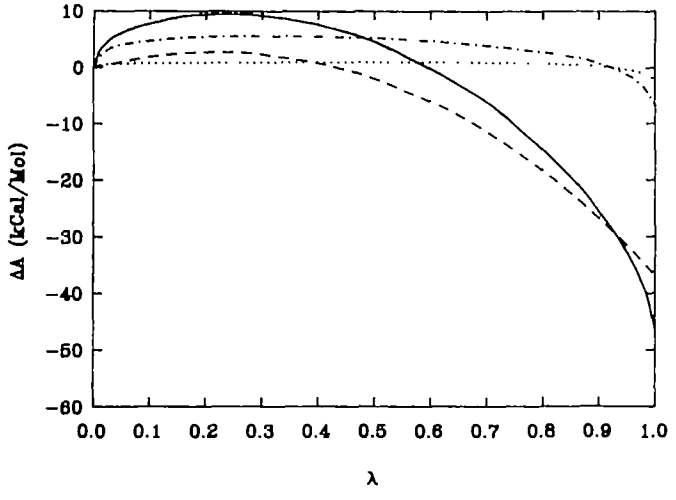

Fig. 5. Helmholtz free energy change for Asn ($\lambda = 0$) to Asp ($\lambda = 1$) mutation of residue 31^L in the unliganded antibody, as a function of the perturbation parameter λ, is indicated by solid line. Its components are also shown as follows: dashed for electrostatic, dash–dotted for covalent and dotted for Lennard–Jones.

free energy is similar in both the Fab–Ag, Fab and Fab* perturbations, it turns out that it largely cancels out in the thermodynamic cycles (see Table III).

The profile of the overall electrostatic contribution to the free energy is approximately quadratic and is similar in both the dipeptide and the protein perturbations.

Contributions from various parts of the system. The contributions to the non-bonded energy arising from various parts of the Fab–Ag and Fab systems are listed in Table IV. Significant residue contributions are grouped into three segments (solvent, antigen and antibody), and among them 'sections' such as complementarity-determining regions CDR_1 and CDR_2, the non-CDR turn of the L chain of the antibody, as well as a strand of the antigen epitope in extensive contact with the mutating residue, labeled 'strand', and the rest of the antigen.

The total non-bonded energy change for the mutation in Table IV is simply taken as the sum of van der Waals and electrostatic energies from Table III. A rapid survey of Table IV shows that the solvent and protein energy terms do not necessarily add up, which results from statistical errors due to insufficient sampling. The following analysis, bearing in mind the large uncertainties associated with these results, adopts a more qualitative approach.

The solvent and Fab contributions differ greatly between the Fab–Ag and the Fab systems. The small contributions to

Table IV. Decomposition of the non-bonded contributions to the Helmholtz free energy changes for $Asn31^L$ to Asp mutation in the HyHEL-10–HEL complex, the unliganded HyHEL-10 antibody and the thermodynamic-cycle perturbation values for columns 2 and 3

			Fab–Ag	Fab	Cycle
Total non-bonded			−44.1	−39.1	−5.0
Solvent			−19.5	−75.1	55.6
Fab			−2.3	36.1	−38.3
	CDR_1		10.8	21.0	−10.2
		Ser28	0.0	5.3	−5.3
		Ile29	−0.2	1.2	−1.4
		Gly30	−0.1	1.8	−1.9
		Asn31	13.7	14.5	−0.8
		Asn32	−3 0	−1.7	−1.3
		Leu33	0.4	−0 1	0.5
	CDR_2		−16.2	3.6	−19.8
		Lys49	3.0	0.3	2.7
		Tyr50	−4.1	4.3	−8.4
		Ala51	−2.9	−1.3	−1.6
		Ser52	−5.2	0.9	−6.1
		Gln53	−7.1	−1.1	−6.0
	Non-CDR		3 2	11.5	−8.3
		Ser65	−0.4	2.0	−2.4
		Gly66	4.6	9.9	−5.3
		Ser67	0.1	0.0	0.1
		Gly68	−0 1	7.6	−7.7
		Thr69	0.0	0.4	−0.4
		Asp70	0.0	3.2	−3.2
		Phe71	−1 1	−1 7	0.6
Ag			−18.6	0.0	−18 6
	Strand		20.1	0.0	20.1
		Ala11	0.6	0.0	0.6
		Met12	1 1	0.0	1.1
		Lys13	1.5	0.0	1.5
		Arg14	9 2	0.0	9.2
		His15	6.3	0.0	6.3
		Gly16	1 3	0.0	1.3
	Other		−38 7	0.0	−38.7
		Asn93	2.0	0.0	2.0
		Lys96	−38.0	0.0	−38.0

All values are in kcal/mol.

the $\Delta\Delta A$ value from the total non-bonded energy thus appear as the result of a balance between solvent and protein terms.

In the complex, the overall antibody term is small, but is itself the balance of large residue contributions that nearly cancel, mainly a large positive term from the mutating residue itself (see Asn31 and CDR_1 values in Table IV) compensated by favorable mid-range electrostatic contributions with nearby CDR_2. Interestingly, the small overall effect of the mutation on the antibody's energy in Fab–Ag correlates with a well-conserved secondary structure and conformation. The antigen contribution is largely favorable to the mutation free energy, arising essentially from the creation of a salt link between $Asp31^L$ and $Lys96^{HEL}$, which was the proposed goal of the point mutation. The strand residues, however, contribute to halving this favorable term. The solvent contribution compares in size with that of Ag, although it amounts merely to one-quarter of its counterpart in the Fab system. This simply reflects the limited access of water molecules to the rim of the Fab–Ag interface.

In the Fab system, by contrast, the solvent is responsible for a very largely favorable contribution to $\Delta\Delta A$, whereas the antibody segment reduces this favorable term by approximately one half. This suggests that whatever protein conformational rearrangements are taking place upon solvation of the antibody surface are driven by the solvent and occur at the expense of protein–protein interactions. Thus, in the Fab system, all three L chain loops near the mutation site appear to oppose the path of the mutation.

We now discuss the contributions of a number of individual amino acid residues and solvent molecules near the site of mutation in relation to the relative energy changes that they induce during the mutation.

The non-bonded contribution from the mutating residue itself, Asn31(L)Asp, is large, positive and nearly identical for both Fab–Ag and Fab systems. Because this side chain was conformationally restrained by construction, because the mutation is practically isosteric, and because the backbone itself retained a consistent conformation at ψ_{31} all along the thermodynamic cycle (see Table I), this large contribution results mainly from the electrostatic repulsion between the new charge and the backbone carbonyl.

Among the other amino acids from CDR_1 of the L chain, Ser28 contributes to the non-bonded energy only in the Fab system. This is because during the mutation, the main chain carbonyl oxygen gets closer to the new Asp charge center by 3 Å.

Similarly, in the unliganded Fab, the ψ backbone transition of $Gly30^L$ results in closer proximity of the carbonyl group of $Gly30^L$ to the mutant group.

Adjacent $Asn32^L$ provides the only other significant term from CDR_1 in the complex. The side chain reorients during the course of the mutation, from (g^-,t) to (g^-,g^-). There is no hydrogen bond formed with the terminal of $Asn31^L$ at any time (it would compete with $Lys96^{HEL}$), but the terminal NH_2 orients in an electrostatically favorable way and ends up within van der Waals contact to the mutant side chain. In the unliganded case, the interaction is purely electrostatic and not as strong because the side chain is kept away by strong hydrogen bonds with the solvent.

CDR_2 of the L chain provides many strong interactions in the complex, but these tend to decrease in magnitude in the unliganded case because the CDR_1 conformation shifts Asn31(Asp) into the solvent somewhat, away from the protein core, decreasing its proximity to CDR_2. This is the case with Lys49, whose carbonyl group points toward the new Asp charge some 5–6 Å away in the complex but is weakened in Fab.

The ring of Tyr50 lies within contact distance of the terminal of $Lys96^{HEL}$. The backbone carbonyl points away from the mutant residue, which makes for a favorable charge–dipole interaction. Inversely, the backbone NH group of $Ala51^L$, whose methyl is in contact with the mutating side chain, points toward the carboxylate of $Asp31^L$, thus providing the other half of that charge–peptide bond stabilization. On the contrary, the peptide bond linking residues 50 and 51 reorients in the wild type solvated Fab so that the carbonyl oxygen of $Tyr50^L$ ends up only 4 Å from the new charge.

In the complex, the backbone NH group of $Ser52^L$ is within 4 Å from $O_{\delta 2}$ of $Asp31^L$. It forms a stable and lasting hydrogen bond with a water molecule which also hydrogen bonds the mutating terminal. This water molecule reorients from hydrogen acceptor to hydrogen donor during the mutation without disrupting its hydrogen bond with $Ser52^L$.

The N_ε atom of $Gln53^L$ lies 5 Å away from the new carboxylate group and donates its hydrogens to two water molecules: the buried water that bridges with $Lys96^{HEL}$ and a surface water which bridges with Asn31(L)Asp.

The backbone carbonyl group of $Gly66^L$ provides the only significant contribution from the non-CDR turn in the Fab–Ag complex. The unfavorable orientation of that group with respect to the charge introduced by the mutation is made possible by the presence of solvent.

In the unliganded Fab case, loop turn reorientations tend to bring CDR_1 and the non-CDR loop closer together. Several large unfavorable energy contributions arise as the non-CDR loop orients its backbone dipoles perpendicularly to the plane of the turn, with peptide carbonyl moieties pointing at the new charge. That is the case for residues 66, 68 and 70.

$Arg14^{HEL}$ is responsible for one of the two large unfavorable terms arising from the 'strand' part of the antigen's epitope. The backbone of $Arg14^{HEL}$, like that of neighboring residues, does not reorient during the mutation. Its carbonyl points straight at the side chain of $Asn31^L$, some 3.5–4.5 Å away. As was the case with $Gln53^L$, this carbonyl forms strong hydrogen bonds with two water molecules that also bind successively to the carboxylate of $Asp31^L$, thus compensating for this large positive energy term.

The carbonyl oxygen of $His15^{HEL}$ forms a strong and stable hydrogen bond with the ammonium group of $Lys96^{HEL}$ < 3 Å away. This also results in its close proximity to the charge created upon mutation.

The side chain carbonyl of $Asn93^{HEL}$ forms stable hydrogen bonds with both the buried water molecule that also binds $Lys96^{HEL}$ and $Gln53^L$ and with the terminal of $Gln53^L$, which locks it into a mildly unfavorable orientation with respect to the mutant side chain.

Finally, the ammonium terminal of $Lys96^{HEL}$ has its charge paired with $Asp31^L$ (N_ε ends up 2.6 Å away from $O_{\delta 1}$), but it also maintains its strong hydrogen bonds throughout the mutation respectively with the backbone oxygens of $Asn31^L$ and $His15^{HEL}$ and with the neighboring buried water (see Figure 3).

This buried water itself contributes little to the mutation free energy, presumably owing to its sideways orientation with respect to the carboxylate. This orientation is well maintained during dynamics because of strong hydrogen bonds with $Lys96^{HEL}$, $Gln53^L$ and $Asn93^{HEL}$, as discussed above.

For illustration, the energetic contributions of two other water molecules that engage in hydrogen bonds with the carboxylate during the course of dynamics in the Fab–Ag system were also computed. The first one also binds $Ser52^L$ and contributes −8.9 kcal/mol to the relative binding free energy of the mutant, while the second one bridges the mutant residue with $Gln53^L$ and contributes −10.2 kcal/mol. The magnitudes of these contributions are comparable to the largest protein residue terms, with the exception of the salt link itself.

Summary. In the antibody–antigen complex, the overall free energy gain arising from the point mutation divides evenly between solvent and antigen contributions, with a marginal contribution from the antibody itself. The latter arises primarily from the near cancellation of a positive mutant self-term with negative contributions from the CDR_2 loop. As to the antigen term, it is dominated by a large salt link term, but tempered by the adverse orientations of backbone carbonyl groups close to the site of mutation.

Out of the 12 protein residues selected as giving significant non-bonded contributions to the free energy change for mutating $Asn31^L$ into Asp in the Fab–Ag complex, one involves a charge–charge term and the other 11 are dominated by charge–dipole interactions: six unfavorable terms with carbonyl groups (five of them on the main chain), one favorable term with a peptide bond and three with uncharged amide or peptide nitrogen groups (two of them in side chains).

As many as five of these residues are involved in hydrogen bonds with waters that also bind the mutant side chain. Among these are residues that contribute large positive energy terms, which the bridging water terms presumably compensate for.

Finally, it seems important to emphasize that all protein contributions to the Fab–Ag free energy change develop in a regular and consistent way throughout the perturbation. This correlates with the consistency of the model throughout the dynamics and with the initial crystallographic data. Thus, there are few backbone reorientations and limited side chain conformational transitions in the Fab–Ag complex, despite the absence of positional or internal constraints inside the dynamical sphere of 30 Å diameter. This solid-like behavior helps in assigning structural origins to the free energy changes and in understanding them from a simple knowledge of the end-points.

In the unliganded Fab mutation, however, more than half a dozen backbone carbonyl groups provide all the large, adverse contributions to the mutation, emphasizing the importance of the CDR and non-CDR loop turns' conformation to the free energy outcome.

Discussion

The present study suggests that the mutation of $Asn31^L$ into Asp in the antibody would lead to a 5.6 kcal/mol stabilization of the HyHEL-10–HEL complex. If confirmed experimentally, this would translate into a 10 000-fold increase in the binding constant. This calculated value seems high, but is off only by an order of magnitude from values observed in another antibody–lysozyme complex (Lavoie *et al.*, 1989) and in an enzyme (Fersht *et al.*, 1985, 1986) upon removal of salt links. In the latter case, Fersht *et al.* (1985, 1986) observed a 1000-fold decrease in enzyme specificity upon unpairing charges in tyrosyl-tRNA synthetase, which corresponds to a destabilization of 4 kcal/mol. This value is, in absolute terms, within the estimated range of error for our calculations.

As far as the structure of antibody–antigen complexes is concerned, the observations made in this study question two assumptions regarding the mechanism of antibody–antigen association. Firstly, the assumption of water exclusion from the interface, since we found that a few water molecules are instrumental in maintaining the crystallographic conformation at the core of the complex, in agreement with recent experimental observations on another HEL antibody complex (Braden and Poljak, 1995). Otherwise, the observations made on the basis of the crystallographic structure are confirmed by simulations of the complex, as far as the nature and detail of contacts involving the antibody L chain CDR loops and the main chain conformation of these regions are concerned.

Secondly, the case for a lock and key association is weakened by the observation of the consistent, if partial, reorientation of a number of peptide bonds of the CDR_2 and the non-CDR loop turns in our model of the unliganded Fab. These findings agree qualitatively with the small but significant CDR conformational changes observed in an important recent study of the association of the antibody Fab 17/9 to a nonapeptide antigen from influenza virus hemagglutinin (Rini *et al.*, 1992 and references therein) and support the possibility of a limited induced-fit in the mechanism of association of antibodies with their antigen (Wilson and Stanfield, 1993).

The approximate decomposition of the free energy changes provides some insight into the free energy change associated with the point mutation. Mark and van Gunsteren (1994) have warned against the overinterpretation of free energy decompositions, since these depend on the path adopted for the perturbation and should therefore be considered in relation to the λ dependence of the Hamiltonian. For their part, Boresch *et al.* (1994) have pointed out that as long as the integration path is taken into account, such decompositions are useful in the interpretation of results, because they shed light on the underlying behavior of the system. In the present study, a cautious approach was adopted. On the one hand, the decomposition by energy type was given for the sake of comparison with the Poisson–Boltzmann electrostatic calculations and in relation to the λ dependence of the Hamiltonian, so as to help evaluate possible sources of error. On the other hand, the analysis by residue was presented in relation to the conformation of the end-points.

Based on such correlation with structural information provided by simulations at the end-points of the thermodynamic cycle, we can attribute the mutation free energy changes to different factors: in the complex, the stabilization of the mutant complex arises from the formation of a salt bridge with $Lys96^{HEL}$, with small or negligible changes due to limited conformational flexibility. Charge formation does not lead to a new, direct hydrogen bond between the charged groups. Instead, $Lys96^{HEL}$ maintains three hydrogen bonds with main chain carbonyl groups and a water molecule. In the unliganded Fab, the solvent Coulombic term was seen to dominate over its protein counterpart because the protein conformation adopted upon full solvation of the Fab was largely unfavorable to the point mutation. The competition of solvent for electrostatic interactions with protein main chain dipoles is well illustrated in this system. The proximity of the solvent stabilizes the charge, but it also forces nearby residues at the surface of the antibody into adopting conformations that destablilize it somewhat.

In short, the enhanced recognition of HEL by the mutant HyHEL-10 appears to arise from the combination of thermo-

dynamically more favorable conformational changes of the CDR loops upon association and subsequent charge pairing in the complex.

Reliable quantitative predictions of the molecular recognition of large substrates using computational tools are seen to depend critically upon a detailed knowledge of the structures at the end-points of the thermodynamic cycle. Obtaining a full cut-off correction to the electrostatic binding energy of flexible systems using continuum electrostatics calculations remains a computationally challenging problem. This may become more feasible with the inclusion of recent developments of the method (Luty *et al.*, 1992). More experimental data are needed to verify the large increase in antibody–antigen affinity one might expect from the calculations reported here upon formation of a salt link between an anti-lysozyme antibody and its antigen. In the future, these could include structural data on unliganded antibodies that may probe the limited extent of conformational rearrangements suggested by our model and thermodynamic studies of site-directed mutants of HyHEL-10. A gene for a single-chain Fv of HyHEL-10 has been synthesized (Tsumoto *et al.*, 1994) and the HyHEL-10 antibody has been expressed in *Escherichia coli* both as a chimeric Fab fragment (K.Patel, S.Smith-Gill and R.C.Willson, unpublished results) and as a single-chain antibody (Neri *et al.*, 1995), making the results of the present study subject to experimental verification. The energetics of HyHEL-10 association with HEL has also been characterized by isothermal titration calorimetry (K.Shick and R.C.Willson, manuscript in preparation).

Acknowledgements

We thank Drs Tjerk Straatsma, Shankar Subramaniam, Rebecca Wade and Martin Zacharias for helpful suggestions. This work was supported in part by grants from NIH, NSF, the Robert A.Welch Foundation, the Human Frontier Science Program and the NSF Supercomputer Centers Metacenter Program.

References

Alzari,P.M., Lascombe,M.-B. and Poljak,R.J. (1988) *Annu. Rev. Immunol*, **6**, 555–580.

Amit,A.G., Mariuzza,R.A., Phillips,S.E.V. and Poljak,R.J (1986) *Science*, **233**, 747–753.

Antosiewicz,J., McCammon,J.A. and Gilson,M.K. (1994) *J. Mol. Biol.*, **238**, 415–436.

Bernstein,F.C., Koetzle,T.F., Williams,G.J.B., Meyer,E.F., Brice,M.D., Rodgers,J.R, Kennard,O., Shimanouchi,T. and Tasumi,M. (1977) *J. Mol. Biol.*, **112**, 535–542.

Beveridge,D.L. and DiCapua,F.M. (1989) *Annu. Rev. Biophys. Biophys. Chem.*, **18**, 431–492.

Boobbyer,D.N A., Goodford,P.J., McWhinnie,P.M. and Wade,R.C. (1989) *J. Med Chem.*, **32**, 1083–1094.

Boresch,S., Archontis,G. and Karplus,M. (1994) *Proteins: Struct. Funct. Genet.*, **20**, 25–33.

Born,M. (1920) *Z. Phys.*, **1**, 45.

Braden,B.C. and Poljak,R.J. (1995) *FASEB J.*, **9**, 9–16.

Brooks,B., Bruccoleri,R.E., Olafson,B., States,D.J., Swaminathan,S. and Karplus,M. (1983) *J. Comput. Chem.*, **2**, 187–217.

Chothia,C. and Lesk,A.M. (1987) *J. Mol. Biol.*, **196**, 901–917.

Dao-Pin,S, Sauer,U., Nicholson,H. and Matthews,B W. (1991) *Biochemistry*, **30**, 7142–7153.

Davis,M.E. and McCammon,J.A. (1989) *J. Comput. Chem.*, **10**, 386–391.

Davis,M.E., Madura,J.D., Luty,B.A. and McCammon,J.A. (1991) *Comp. Phys. Commun.*, **62**, 187–197.

Dill,K.A. (1990) *Biochemistry*, **29**, 7133–7155.

Fersht,A.R., Shi,J.-P, Knill-Jones,J., Lowe,D.M., Wilkinson,A.J., Blow,D M., Brick,P., Carter,P., Waye,M.M.Y. and Winter,G. (1985) *Nature*, **314**, 235–238.

Fersht,A.R., Leatherbarrow,R.J. and Wells,T.N.C. (1986) *Phil. Trans. R. Soc. Lond.*, **A317**, 305–320.

Gilson,M.K., Sharp,K.A. and Honig,B.H. (1987) *J. Comput. Chem.*, **9**, 327–335.

Goodford,P.J. (1985) *J. Med. Chem.*, **28**, 849–857.

Honig,B.H., Sharp,K.A. and Yang,A.-S. (1993) *J. Phys. Chem.*, **97**, 1101–1109.

Horovitz,A., Serrano,L., Avron,B., Bycroft,M. and Fersht,A.R. (1990) *J. Mol. Biol.*, **216**, 1031–1044.

Jorgensen,W.L., Chandrasekhar,J., Madura,J.D., Impey,R.W. and Klein,M.L. (1983) *J. Chem. Phys.*, **79**, 926–935.

Komeiji,Y., Uebayasi,M., Someya,J. and Yamato,I. (1992) *Protein Engng*, **5**, 759–767.

Kuczera,K., Gao,J., Tidor,B. and Karplus,M. (1990) *Proc. Natl Acad. Sci. USA*, **87**, 8481–8485.

Lavoie,T.B. *et al.* (1989) In Smith-Gill,S.J. and Sercarz,E. (eds), *The Immune Response to Structurally Defined Proteins: The Lysozyme Model*, Adenine Press, New York, pp. 151–168.

Lee,C. (1992) *Curr. Opin. Struct. Biol.*, **2**, 217–222.

Luty,B.A., Davis,M.E. and McCammon,J.A. (1992) *J. Comput. Chem.*, **13**, 768–771.

McCammon,J.A. and Harvey,S.C. (1987) *Dynamics of Proteins and Nucleic Acids*. Cambridge University Press, Cambridge.

Mark,A.E. and van Gunsteren,W.F. (1994) *J. Mol. Biol.*, **240**, 167–176.

Meyer,E. (1992) *Protein Sci.*, **1**, 1543–1562.

Neri,D., Momo,M., Prospero,T. and Winter,G. (1995) *J. Mol. Biol.*, **246**, 367–373.

Novotny,J., Bruccoleri,R.E. and Saul,F.A. (1989) *Biochemistry*, **28**, 4735–4749.

Padlan,E.A., Silverton,E.W., Sheriff,S., Cohen,G.H., Smith-Gill,S.J. and Davies,D.R. (1989) *Proc. Natl Acad. Sci. USA*, **86**, 5938–5942.

Pearlman,D.A. and Kollman,P.A. (1991) *J. Chem. Phys.*, **94**, 4532–4545.

Pearson,R.G. (1986) *J. Am. Chem. Soc.*, **108**, 6109–6114.

Pomès,R. (1993) PhD thesis, University of Houston.

Pomès,R. and McCammon,J.A. (1990) *Chem. Phys. Lett.*, **166**, 425–428.

Presta,L.G. (1992) *Curr. Opin. Struct. Biol.*, **2**, 593.

Prevost,M., Wodak,S.J., Tidor,B. and Karplus,M. (1991) *Proc. Natl Acad. Sci. USA*, **88**, 10880–10884.

Rini,J.A., Schulze-Gahmen,U. and Wilson,I.A. (1992) *Science*, **255**, 959–965.

Roush,D.J., Gill,D.S. and Willson,R.C. (1994) *Biophys. J.*, **66**, 1290–1300.

Sauer,R.T. and Lim,W.A. (1992) *Curr. Opin. Struct. Biol.*, **2**, 46.

Schiffer,M., Chang,C., Naik,V. and Stevens,F.J. (1988) *J. Mol. Biol.*, **203**, 799–802.

Sharp,K.A. and Honig,B.H. (1990) *Annu. Rev. Biophys. Chem.*, **19**, 301–332.

Shen,J., Subramaniam,S., Wong,C.F. and McCammon,J.A. (1989) *Biopolymers*, **28**, 2085–2096.

Sheriff,S., Silverton,E.W., Padlan,E.A., Cohen,G.H., Smith-Gill,S.J., Finzel,B. and Davies,D.R. (1988) In Sarma,R.H. and Sarma,M.H. (eds), *Structure and Expression. Volume 1. From Proteins to Ribosomes*. Adenine Press, New York, pp. 49–53.

Slagle,S.P., Kozack,R.E. and Subramaniam,S. (1994) *J. Biomol. Struct. Dyn.*, **12**, 439–456.

Smith-Gill,S.J., Lavoie,T.B. and Mainhart,C.R. (1984) *J. Immunol.*, **133**, 384–393.

Straatsma,T.P. and Berendsen,H.J.C. (1988) *J. Chem. Phys.*, **89**, 5876–5886.

Straatsma,T.P. and McCammon,J.A. (1989) *J. Chem. Phys.*, **90**, 3300–3304.

Straatsma,T.P. and McCammon,J.A. (1991) *Methods Enzymol.*, **202**, 497–511.

Straatsma,T.P. and McCammon,J.A. (1992) *Annu. Rev. Phys. Chem.*, **43**, 407–435.

Straatsma,T.P., Zacharias,M. and McCammon,J.A. (1992) *Chem. Phys. Lett.*, **196**, 207–302.

Subramaniam,S., McCammon,J.A. and Bacquet,R.J. (1989) In Smith-Gill,S.J. and Sercarz,E. (eds), *The Immune Response to Structurally Defined Proteins: The Lysozyme Model*. Adenine Press, New York, pp. 169–176.

Tembe,B.L. and McCammon,J.A. (1984) *Comput. Chem.*, **8**, 281–283.

Tidor,B. and Karplus,M. (1991) *Biochemistry*, **30**, 3217–3228.

Tsumoto,K., Ueda,Y., Maenaka,K., Watanabe,K., Ogasahara,K., Yutani,K. and Kumagai,I. (1994) *J. Biol. Chem.*, **269**, 28777–28782.

van Gunsteren,W.F. and Berendsen,H.J.C. (1990) *Angew. Chem. Intl Ed. Engl.*, **29**, 992–1023.

Wade,R.C., Mazor,M.H., McCammon,J.A. and Quiocho,F.A. (1990) *J. Am. Chem. Soc.*, **112**, 7057–7059.

Wade,R.C., Mazor,M.H., McCammon,J.A. and Quiocho,F.A. (1991) *Biopolymers*, **31**, 919–931.

Warwicker,J. and Watson,H.C. (1982) *J. Mol. Biol.*, **157**, 671–679.

Wilson,I.A. and Stanfield,R.L. (1993) *Curr. Opin. Struct. Biol.*, **3**, 113–118.

Received October 23, 1995; revised April 20, 1995; accepted May 8, 1995